

The jets of quasar 1928 + 738: superluminal motion and large-scale structure

C.A. Hummel^{1,7}, C.J. Schalinski^{1,2}, T.P. Krichbaum¹, M.J. Rioja^{1,3}, A. Quirrenbach^{1,7}, A. Witzel¹, T.W.B. Muxlow⁴, K.J. Johnston⁵, L.I. Matveyenko⁶, and A. Shevchenko⁶

¹ Max-Planck-Institut für Radioastronomie, Auf dem Hügel 69, W-5300 Bonn 1, Federal Republic of Germany

² Geodätisches Institut der Universität Bonn, Nußallee 17, W-5300 Bonn 1, Federal Republic of Germany

³ Instituto de Astrofísica de Andalucía, Apartado 2144, E-18080 Granada, Spain

⁴ Nuffield Radio Astronomy Laboratories, Jodrell Bank, Macclesfield, Cheshire SK11 9DL, United Kingdom

⁵ Center for Advanced Space Sensing, Naval Research Laboratory, Washington, D.C. 20375, USA

⁶ Space Research Institute, Academy of Sciences of the USSR, Profsojuznaja 84/32, Moscow 117 810, USSR

⁷ Now at NRL/USNO Optical Interferometer Project and Universities Space Research Association (USRA)

Received March 8, accepted September 8, 1991

Abstract. The two-sided radio structure associated with the S5-quasar 1928 + 738 ($z=0.30$) has been mapped at 408 and 1662 MHz with MERLIN, at resolutions of 1.5 and 0.2 arcsec, respectively. We investigate a geometrical and kinematical description of the curved jets in terms of a precessing beam model; moderate intrinsic brightness asymmetry of the jets has to be invoked to account for the apparent brightness ratio of jet to counterjet. This comparatively low ratio seems to contradict the existence of a one-sided milliarcsecond scale jet that has been reported to display superluminal motion. The mas scale jet structure may consist of boosted filaments embedded in a broad cylindrical jet.

The results of five years' monitoring of the radio structure at 22 GHz with VLBI – at the highest angular resolution obtained for this source so far – display ballistic superluminal motion along a sinusoidally curved jet ridge line. Amongst three possible interpretations for this phenomenon, namely orbital motion of the central engine in a binary black hole system – which also could be responsible for the hypothetical precession, Kelvin–Helmholtz instabilities, or a helical magnetic field structure attached to a rotating accretion disk, only the last one might provide a realistic explanation of the observed phenomenon. The apparent velocity of the components observed at 22 GHz (4.0c) is significantly lower than that observed at 5 GHz (6.5c) further down the jet by Witzel et al. (1988).

Key words: quasars: individual – quasars: jets of

1. Introduction

Models explaining large-scale curvature of jets of extragalactic radio sources fall into two varieties, those invoking jet ejection with variable position and direction, and those invoking interactions of the jet with the ambient medium. The first class of

model includes orbital motion (e.g. 3C 449: Lupton & Gott 1982) and jet precession (e.g. Gower et al. 1982), resulting in jet geometries showing mirror and inversion symmetry, respectively. Combinations of these effects can be present in more complex structures. The second class of model includes Kelvin–Helmholtz instabilities (e.g. 3C 449: Hardee 1981), jet deflection by clouds via oblique shock formation (e.g. 3C 388: Burns & Christiansen 1980; 3C 205: Lonsdale & Barthel 1984; Henriksen 1984), and jet bending by ram pressure resulting from motion through cluster gas (head–tail sources: e.g. NGC 1265: O'Dea & Owen 1987; O'Donoghue et al. 1990) or pressure gradients (e.g. 3C 293: Henriksen et al. 1981; Fiedler & Henriksen 1984).

The precessing beam model has been used to explain curved jet structures on the milliarcsecond (mas) scale as well. This model clearly leads to very short precession periods, of the order of several hundred years (e.g. 0153 + 744: Hummel et al. 1988). Begelman et al. (1980) suggested that jet precession might be driven by geodetic precession of the rotation axis of the central hypothetical black hole in a close binary system of these super-massive compact objects. Small-scale transverse oscillations of the order of the binary separation should then be found in very high resolution VLBI (very long baseline interferometry) maps of the jets emerging from the central engine. The lifetime of such a close binary is very short owing to gravitational radiation, so that these objects may be seen in a final short-lived and violent phase (Roos 1988).

The curvature, transverse displacements and spatial oscillations of jet ridge lines observed on mas scales might alternatively be explained in terms of the interaction of the jets with the ambient medium leading to various modes of the Kelvin–Helmholtz instability. Whereas the fundamental helical mode, involving the whole jet, tends to disrupt it through the formation of oblique reflection shocks (Hardee & Norman 1989), helical modes can produce ridge line oscillations within the boundary of a jet (e.g. 3C 345: Hardee 1987). Additionally, specific magnetic field configurations (see Sect. 3.6) might be the cause of quasisinusoidal oscillations of the jet ridge line. Thus, these models imply that the structures seen by means of VLBI are bright features (filaments of a beam) in a broad (possibly straight) jet which is invisible because of the limited dynamic range of the maps. The

Send offprint requests to: C.A. Hummel
U.S. Naval Observatory, AD5, Bldg. 52
34th & Massachusetts Avenue, NW
Washington, DC 20392-5100

envelope of the filaments, however, should outline the arcsecond scale jet. To test this hypothesis, it is important to obtain maps of the jet in the transition region from mas scales to arcsecond scales at high resolution and dynamic range, since at this scale we can relate the observed structures to the ones observed both on smaller and on larger scales. Complementary kinematical information about components moving along the jet, observed by VLBI on mas scales, may help to discriminate between the various models.

In this paper, we address these questions for the case of the quasar 1928+738, which is one of the best studied sources in a complete sample of extragalactic flat spectrum radio sources taken from the S5 strong source survey (Kühr et al. 1981; Witzel 1987). Throughout this paper, we will use $H_0 = 100 \text{ km s}^{-1} \text{ Mpc}^{-1}$, $q_0 = 0.5$. 1928+738 has been reported by Eckart et al. (1985) to display superluminal motion with a mean velocity of $7c$. It has a redshift of 0.30 (Lawrence et al. 1986, 1987) and a bolometric ($400 \text{ MHz} - 2 \cdot 10^{14} \text{ Hz}$) luminosity in the extended lobes of $\approx 5 \cdot 10^{42} \text{ erg s}^{-1}$. The luminosity distance is 960 Mpc. One second of arc corresponds to 2.8 kpc at the distance of the quasar; an apparent motion of 1 mas yr^{-1} corresponds to a transverse velocity of $12c$.

The radio observations will be presented in Sect. 2. In Sect. 2.1, we show a high dynamic range map of the large-scale structure of 1928+738 at 408 MHz, obtained with the MERLIN interferometer, which complements the map obtained with the VLA at 1.5 GHz by Johnston et al. (1987) at a similar resolution. VLBI monitoring observations at 22 GHz are reported in Sect. 2.2. In Sect. 3, the curved radio jet displayed in the maps of the large-scale structure of 1928+738 is discussed primarily in terms of a precessing beam model, but other scenarios are also considered. We compare this model with the VLBI observations of the mas scale radio jet. The kinematics of components in the mas scale jet displaying small-scale oscillations are also discussed.

2. Radio observations and results

2.1. Observations of the kpc scale structure

Figure 1 shows a map of 1928+738 (with our precessing beam model superimposed; see Sect. 3.1), obtained with the VLA in the A configuration on October 31, 1983, at 20 cm wavelength by Johnston et al. (1987). A bright core emits two oppositely directed, strongly bent jets, the northern one pointing towards a large diffuse lobe. The southern, more prominent, jet ends in the vicinity of a low surface brightness, diffuse area of emission to the southwest which is seen in a VLA-B image at 18 cm by Rusk & Rusk (1986) (Fig. 2). This area of emission can be interpreted as the southern lobe, because it is located opposite to the northern one, at about the same distance from the core. To illustrate our interpretation, we have put circles around the bulk of the emission in the northern and southern lobes in Figs. 1 and 2. The northern circle is centered on the brightness maximum of the northern lobe in Fig. 2 and the southern circle is located on the opposite side at the same distance from the core. The source is embedded in a faint halo of emission. The overall projected extent of 1928+738 is $\approx 220 \text{ kpc}$; the real size is probably much larger, since the inclination to the line of sight (LOS) is unlikely to be large, as is indicated by the large apparent jet curvature, the small lobe-core separation and the one-sided pc-scale jet (see next section) pointing towards the south.

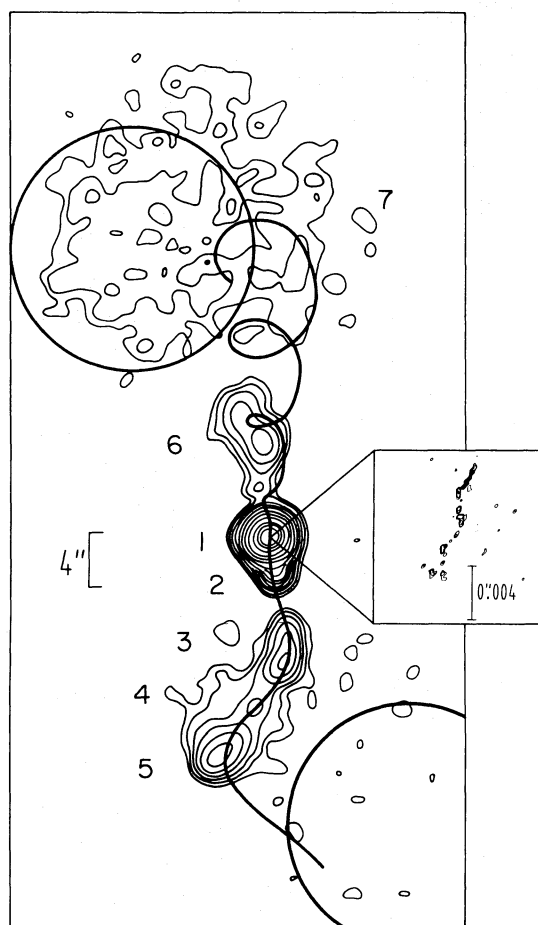


Fig. 1. VLA (A configuration) map of 1928+738 at 20 cm wavelength (Johnston et al. 1987; same description of the components) with the precessing beam model superimposed. The restoring beam is a 1.8 by 1.6 arcsec Gaussian at a position angle of $\phi = -62^\circ$. Contour levels are $-0.53, 0.53, 0.84, 1.3, 2.1, 3.4, 5.3, 8.4, 13, 21, 34, 53, 84, 133, 211, 335, 531, 842, 1223$ and 2114 mJy/beam . Model parameters are: $i = 43^\circ$, $\psi = 8^\circ$, $\phi = 230^\circ$, $\beta = 0.7$ and $P = 430\,000 \text{ yr}$ (see Sect. 3.1). The inset shows the VLBI 1.3 cm “delta” map of epoch 1988.73 (relative magnification 4000:1), and is intended to show the relative magnitude of transverse jet oscillations due to precession (arcsecond scales) and orbital motion (mas scales). Note that all observed VLBI components are south of the central compact source. Circles are placed at the same position as in the map by Rusk & Rusk (1986), shown in Fig. 2

On October 27, 1987, the source was observed with the MERLIN interferometer (stations Lovell, Tabley, Darnhall, Wardle, Knockin and Defford) at 408 MHz (10 MHz bandwidth) for 17 h. The resulting map, obtained using the OLAF hybrid mapping package, has a resolution similar to that of the VLA map at 20 cm (1.5 arcsec) and is shown in Fig. 3a.

In order to calculate the spectral indices of the individual components, we summed the flux density at 408 MHz within small boxes containing the component (AIPS tasks IMEAN and IMFIT) and in addition fitted Gaussian component models to the data (Caltech VLBI software, task MODELFIT). The results were consistent except for component 6, which seems to be slightly resolved since MODELFIT tends to put a more extended component at that position with more flux density (54 mJy). However, we used the IMEAN value (40 mJy) since the same

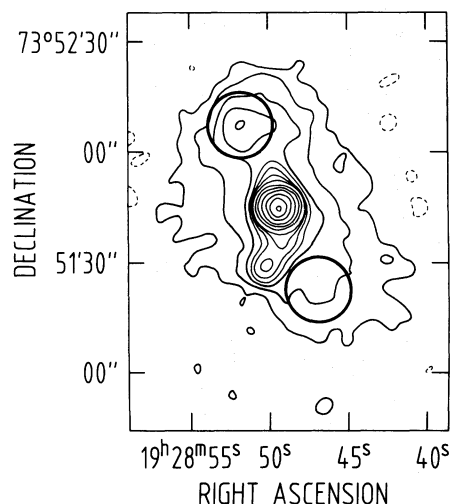


Fig. 2. VLA (B configuration) map of 1928+738 at 18 cm wavelength (Rusk & Rusk 1986). Restoring beam is a 5 arcsec circular Gaussian. Contour levels are $-0.034, 0.034, 0.10, 0.20, 0.30, 0.40, 0.60, 1.0, 3.0, 5.0, 10, 30, 50$, and 95% of the peak flux density of 2.97 Jy/beam. Circles superimposed on the lobes are symmetrically placed with respect to the core

method has been used to derive flux densities of the components in the VLA map by Johnston et al. (1987) (note that the flux density given for component 6 by Johnston et al. is erroneously low by a factor of 2). Additionally, we graphically integrated the contours of a map made at 6 cm with the VLA by Kollgaard et al. (1990). Although the component flux densities obtained in this way are less accurate, we did check that the integrated flux density of the southern jet is consistent with the value given by the authors. Component 6, for which Kollgaard et al. (1990) do not give a flux density, is sufficiently detached from the core at the resolution of 3.5 arcsec of their map that we have been able to determine a flux density by graphical integration. An estimate for the 6 cm flux density of component 2 was derived by graphical integration of maps made by Rusk & Rusk (1986) with the VLA in the B configuration (R. Rusk, priv. comm.), which have slightly higher (uniform weighting of data) or similar (natural weighting) resolution to that of the 20 cm A-configuration map. The results are listed in Table 1. Errors in the spectral indices based on empirical estimates are about ± 0.1 (± 0.2 in the case of graphically integrated component flux densities).

On October 31, 1989, 1928+738 was observed with MERLIN (seven stations, including Cambridge) at 18 cm for 12 h. The resulting map is shown in Fig. 4 and shows the inner few

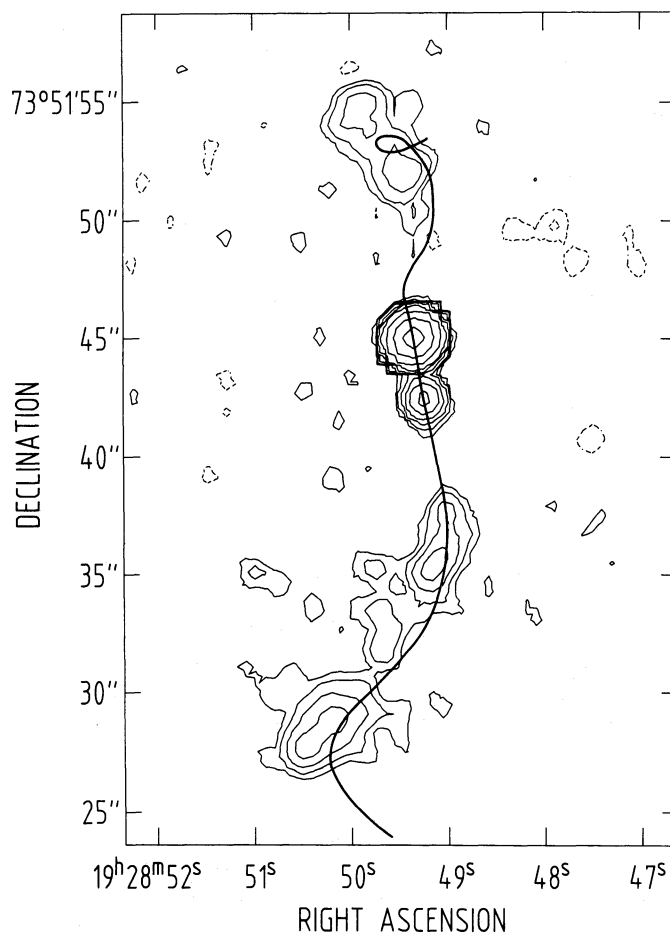
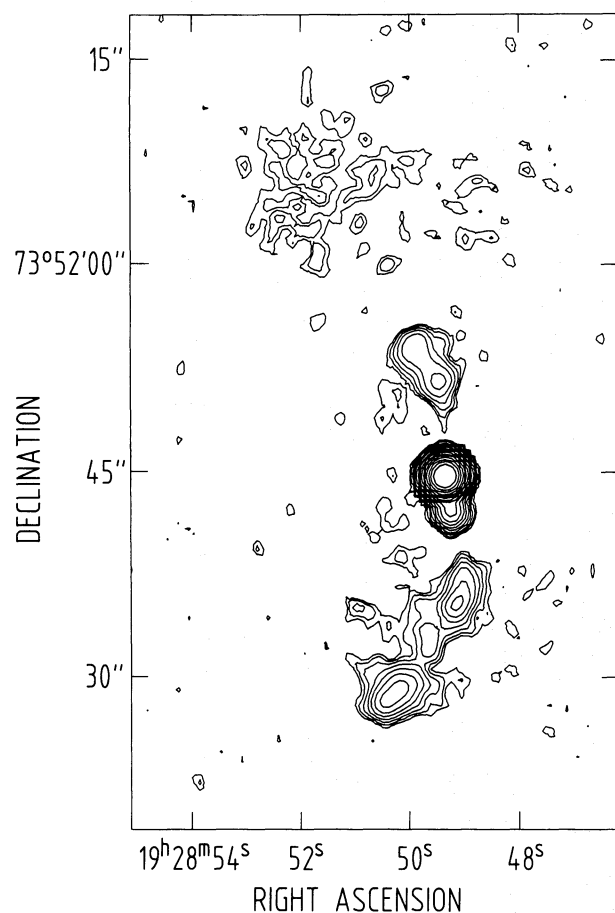


Fig. 3. a MERLIN 408 MHz map. Restoring beam is a 1.5 arcsec circular Gaussian. Contour levels are $-1.4, -0.9, 0.9, 1.4, 2.3, 3.6, 5.7, 9.0, 14.3, 22.6, 35.8, 56.8, 90.0, 142, 226, 358, 568, 900, 1426$ mJy/beam (2 db intervals). Peak flux density is 3.55 Jy/beam. **b** MERLIN 408 MHz map at 1 arcsec resolution. Contour levels are $-2, -1, 1, 2, 4, 8, 16, 32, 128, 512, 2048$ mJy/beam. The locus of the trajectories of components moving according to a precessing beam model with decreasing velocity is superimposed on the map (see Sect. 3.1)

Table 1. Components of 1928 + 738

Component	$S_{408\text{ MHz}}$ (mJy)	$S_{1.5\text{ GHz}}$ (mJy)	$S_{5\text{ GHz}}$ (mJy)	$\alpha_{408\text{ MHz}}^{1.5\text{ GHz}}$	$\alpha_{1.5\text{ GHz}}^{5\text{ GHz}}$
1	3550	3350	2776	0.0	-0.2
2	45	16	7 ± 2	-0.8	-0.7 ± 0.2
3+4	46	21	17	-0.6	-0.2
5	64	19	13	-0.9	-0.3
6	40	18	8 ± 2	-0.6	-0.7 ± 0.2
7	—	111	40	—	-0.9

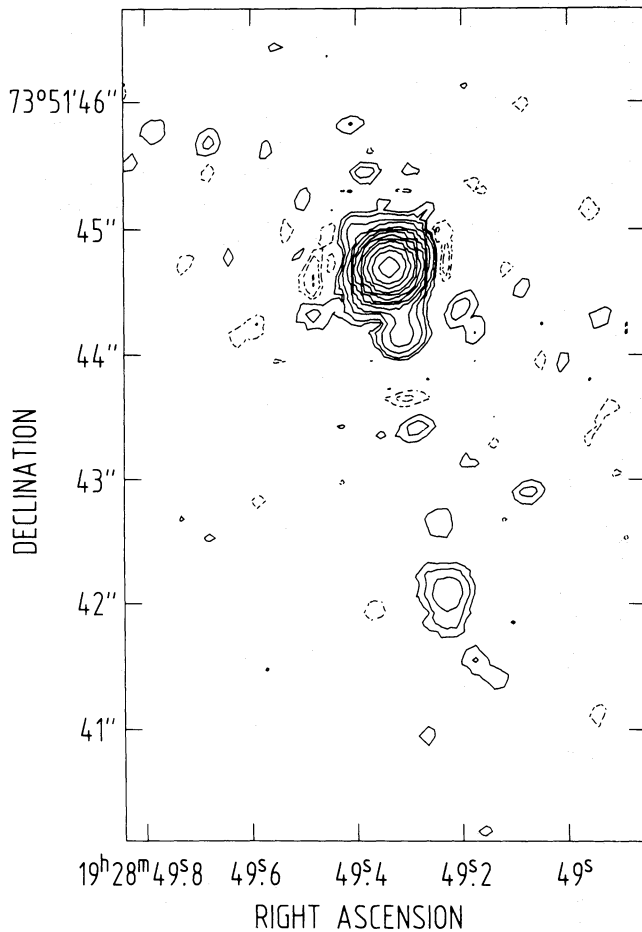


Fig. 4. MERLIN 18 cm map. Restoring beam is 0.2 arcsec. Contour levels are -2, -1, -0.5, 0.5, 1, 2, 4, 8, 16, 32, 64, 128, 256, 512, 1024, 2048 mJy/beam. Peak flux density is 3.6 Jy/beam

arcseconds of the jet near the core, at a resolution of 0.2 arcsec. Component 2 (11 mJy) is seen at a distance of 2670 ± 40 mas to the south of the core, while another component with a flux density of 10 mJy can also be seen in the same direction but with a separation of 540 ± 40 mas from the core. The three components defining the jet to the south are well aligned at position angle 190° , suggesting that the jet is straight at least over the first 3 arcsec of its trajectory.

2.2. Observations of the pc scale structure

VLBI observations at 6 cm wavelength show that, on a mas scale, 1928 + 738 displays a one-sided core-jet structure (at the dynamic range of $\approx 100:1$ of the maps). The jet contains components moving southward away from the core with a common velocity of $\approx 6c$ (Witzel et al. 1988). New VLBI maps of this quasar have been made at wavelengths of 90, 50, 18, and 6 cm and are discussed by Schalinski (1990).

For the 1.3 cm observations presented in this paper, we used the Mark III VLBI system in Mode B (28 MHz recording bandwidth) at epochs 1985.10 and 1986.40, and the Mark II system with 1.8 MHz bandwidth at the subsequent epochs. The source was observed continuously for 12 to 15 h at each epoch, except for 1985.10 (7 min observation per 15 min) and 1986.40 (7 min per 30 min due to switching with another source). Five to eight stations were involved at each epoch (see Table 2). The aperture plane coverage of epochs 1986.40 and 1987.44 was significantly worse than at the other epochs and resulted in higher sidelobe levels and lower quality for the corresponding maps. As a measure of this, we list in Table 2 the number of baseline-hours observed and the minimum and maximum sidelobe levels and widths of the synthesized beams.

All the data were correlated at the MPIfR in Bonn. In cases when it was difficult to obtain fringes, a global fringe fitting algorithm developed by Alef and Porcas (1986) was used. For the MK II observations, the signal from the source was detected reliably only on the baselines to Effelsberg, and on most continental US-baselines, so that these baselines provided the estimates of the interferometer delays and fringe rates for all other baselines. The global fringe fitting procedure then gave more useful data and a significantly enhanced quality of the measured closure phases. The data were calibrated using measured values of the system temperatures and gains (sensitivities) of the participating telescopes. Relative adjustments to the station gain factors, which deviated from the values provided by the station log sheets by up to 40%, were derived for the epochs 1988.73, 1989.25 and 1989.71 from 20-min observations of the BL Lac object 1803 + 78 (≈ 3 Jy). At 3.6 cm, this compact source essentially consists of two stationary components 1.4 mas apart, showing a brightness ratio of roughly ten to one (Witzel et al. 1988). At 1.3 cm, 1803 + 78 shows a modulation of the visibility amplitude which increases from less than 10% on baselines shorter than 50 million wavelengths to a maximum of $\approx 50\%$ on baselines of 250 million wavelengths. On even longer baselines, the modulation decreases owing to the increasing dominance of the very compact core component [see Krichbaum (1990a)]. The envelope of the maximum visibilities

Table 2. VLBI observations of 1928+738 at 22.2 GHz

Epoch	Stations ^a	Obs. time ^b (h)	Sidelobe level min., max. (%)	Beam shape ^c (mas)	p.a. ^d (°)	<i>S</i> (Jy)	Visibility ^e	<i>T_B</i> (10 ¹² K)
1985.10	BSGKO	45	−20, 15	0.24 × 0.21	−16	2.4	0.83	0.05
1986.40	BSGKYO	14	−15, 35	0.30 × 0.20	−67	2.4	0.87	0.11
1987.44	BSLGKYO	47	−15, 25	0.45 × 0.21	−45	2.6	0.84	0.11
1988.73	BSLRGKYO	70	−15, 15	0.27 × 0.18	−37	2.9	0.83	0.09
1989.25	BLRGKVO	89	−20, 20	0.27 × 0.17	4	3.1	0.87	0.10
1989.71	BSGKVPYO	195	−15, 15	0.22 × 0.21	−27	3.4	0.68	0.07

^a Station keys and information(All stations were equipped with H Masers. Coherence times were typically 60 to 120 s. System temperatures *T_{sys}* (K) and corrected gains (K/Jy) are mean values of the last observing epoch at which the station participated)

Key	Station	Diam. (m)	<i>T_{sys.}</i>	Gain
B	Max-Planck-Institut für Radioastronomie, Effelsberg, FRG	100	170	0.44
S	Onsala Space Observatory, Onsala, Sweden	20	310	0.056
L	Istituto di Radioastronomia, Medicina, Italy	32	230	0.043
R	Crimean Astrophysical Observatory, Simeiz, USSR	22	160	0.04
G	National Radio Astronomy Observatory (NRAO ¹), Green Bank, WV	43	200	0.05
K	Haystack Observatory, Westford, MA	37	130	0.10
V	NRAO, Pie Town, NM	25	70	0.11
P	NRAO, Kitt Peak, AZ	25	140	0.11
Y	NRAO VLA, Socorro, NM (in 1989.71 phased array of 27 antennas)	25	200	1.35
O	Owens Valley Radio Observatory, Big Pine, CA	40	90	0.08

¹ The National Radio Astronomy Observatory is operated by Associated Universities, Inc., under cooperative agreement with the National Science Foundation of the USA^b Total number of baseline-hours observed. In 1986.40, the source was observed in a 30-min switching cycle. Note that due to the high declination of the source, the uv coverage was typically of circular shape (except in 1987.44)^c Major and minor axis of the central elliptical Gaussian component of the synthesized antenna beam, assuming uniform weighting. Note that a circular beam was actually used to restore the maps of Fig. 5^d Position angle of the major axis of the beam shape^e Visibility (compactness) defined as ratio of detected peak flux density on shortest baseline (equal to the total flux contained in the map) to total flux density *S* as measured by a single telescope

plotted versus the baseline length is to a good approximation Gaussian up to lengths of 500 million wavelengths. We assumed this behaviour to be valid at the last three epochs of our monitoring program. Thus, the structural information on 1803+78, when necessary, was used to extrapolate the measured visibility amplitude on a baseline to its maximum value it would have attained if the calibrator had been observed continuously. A Gaussian curve was fitted to the (extrapolated) visibility amplitudes versus projected baseline length, and station gain factor corrections were derived from the deviations of the visibilities from the curve on the assumption that the visibilities are directly dependent on the product of the gain factors of the two stations involved. The width of the Gaussian curve, initially fitted to the uncorrected data, was adjusted to give the smallest scatter of the corrected visibilities around the curve. In 1987.44, the very compact quasar 0016+73 (≈ 2 Jy) was used as a calibrator. The flux density scale of the calibration was set by the condition that the correlated flux density of the compact calibrator should equal the single dish flux density, as measured at Effelsberg at the epoch

of the VLBI observation. At the other epochs where no calibrator was observed, we fixed the geometric mean of the station gain corrections (determined in the process of mapping by time independent amplitude self-calibration) in order to prevent the flux density scale from floating. Although the calibration of a VLBI array at such high frequencies is strongly affected by weather, we empirically estimate the absolute accuracy of our flux densities to be better than $\approx 15\%$. Standard image reconstruction algorithms for aperture synthesis data including phase self-calibration were then used for mapping (a point source model was used as a starting model in each epoch). Time dependent amplitude self-calibration was not found to be necessary for most of the stations at any epoch.

Figure 5 shows the maps at 1.3 cm, restored with a beam of 0.25 mas (an identification of the components is indicated: see Sect. 3.3). They show a bright, pronounced jet, exhibiting regular transverse oscillations. This phenomenon has not previously been observed in this source, since the scale of these oscillations is too small to be detected in maps of the jet structure that have been

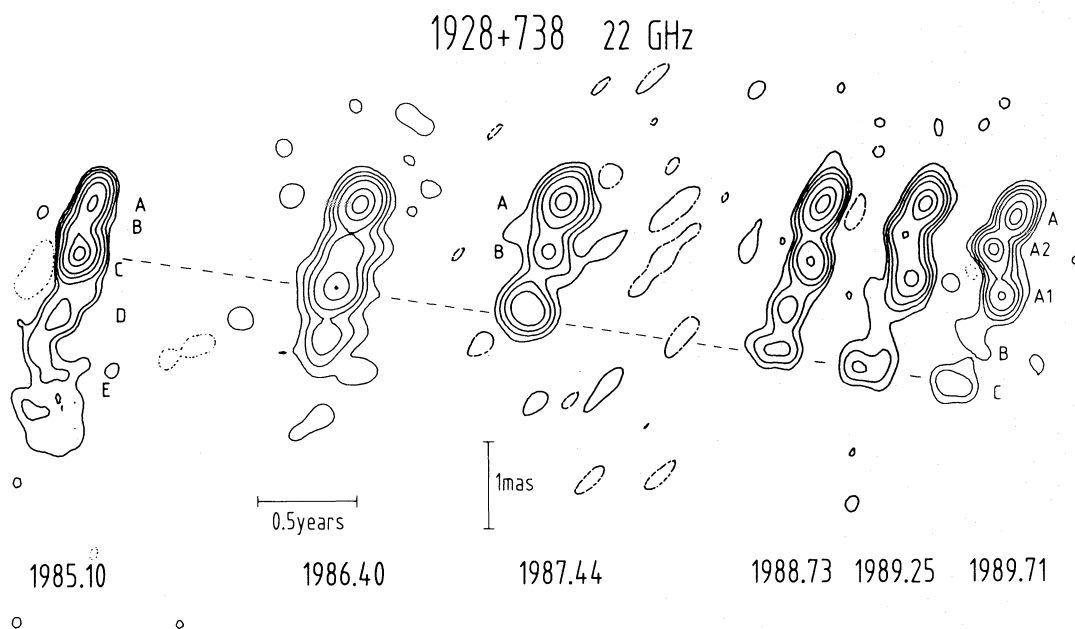


Fig. 5. Display of the maps obtained by VLBI observations of 1928 + 73 at 1.3 cm wavelength at epochs (from left to right) 1985.10, 1986.40, 1987.44, 1988.73, 1989.25, and 1989.71. Contour intervals (in % of the peak brightness; negative contours dashed) are: 1985.10: -3, 3, 5, 10, 20, 30, 50, 80; 1986.40: -5, 5, 10, 20, 30, 50, 80; 1987.44, 1988.73 and 1989.25: -2, 2, 5, 10, 20, 50, 80. Restoring beam width is 0.25 mas for all epochs (except 1987.44 and 1986.40: 0.3 mas); synthesized interferometer beam widths are given in Table 2. The identification of component (C) is indicated by a dashed line; see Sect. 3.2

made at 6 cm wavelength (notwithstanding quite complex structures of the jet on scales of several mas). The observed visibilities were modeled with a set of Gaussian components (MODELFIT) in order to obtain physically meaningful parameters, such as the component diameters, flux densities and positions. The results are given in Table 3; col. 1 gives the component identification, col. 2, the flux density (errors typically about 15%), col. 3, the distance from the core (comp. A), col. 4, errors of the distances, col. 5 (and 6), the position angle (and error) with respect to the core, col. 7, the size, col. 8, the position angle of the major axis, and col. 9, the epoch of observation. Errors were estimated empirically during the process of model fitting.

3. Discussion

3.1. A precessing beam model for the arcsecond scale jet

The general structure of the quasar 1928 + 738, as indicated by the circles in Fig. 1, can be considered to be of the classical symmetric double type, because the lobes are collinear with the core and are located about the same distance on either side of the core. Since the lobes are the oldest components in the structure, we conclude that no obvious distortions resulting from ram pressure arising from motion through an intergalactic medium are present in the core-lobe structure.

Using an iterative procedure to solve the set of non-linear equations given by Gower et al. (1982), we calculated a family of “simple” precessing beam models within a range of parameter values, which all give satisfactory fits to the observed jet line. The best fitting model is superimposed on the VLA map in Fig. 1. It fits the southern jet quite well, and the northern jet (component 6) relatively well. To the south the model jet line ends up roughly in the southern lobe, whereas to the north the projected model line

shows large twists at the position of the lobe. The parameters of the model are given in the figure caption. Allowed ranges for the parameters are as follows (but note that not all combinations are allowed): inclination of the cone axis to the line of sight (LOS) $40^\circ \leq i \leq 50^\circ$, half cone opening angle $8^\circ \leq \psi \leq 10^\circ$, azimuth angle $200^\circ \leq \varphi \leq 230^\circ$, intrinsic velocity $0.7 \leq \beta \leq 0.8$, precession period $380\,000 \text{ yr} \leq P \leq 430\,000 \text{ yr}$. The position angle of the cone axis in the plane of the sky is $\approx 180^\circ$. The precession is clockwise in these models, as seen from the observer. Models with counterclockwise precession and the same parameter values besides an azimuth angle of $180^\circ - \varphi_{\text{clockwise}}$ also give a good fit to the data.

Since the jet velocity β of the model is 0.7, noticeable relativistic effects must occur. Assuming that the intrinsic lengths of the jet and counterjet (taken as the separations of components 5 and 6 from the core, respectively) are the same, the ratio f of the apparent distances to the core on the jet and counterjet side (south and north) is about 1.7 and is given by

$$f = \left(\frac{1 + \beta \cos i}{1 - \beta \cos i} \right).$$

From that we calculate a jet to counterjet brightness ratio $f^{2-\alpha}$ of about 4 (α taken as -0.6). Out to a distance of 2 arcsec from the core, the *measured* ratio (peak brightness ratio) is 10, which drops to 3 if the integrated jet flux densities (component 6, and components 2, 3, 4, and 5) are considered (Johnston et al. 1987). Thus there is evidence for relativistic motion in the jets on the kpc scale. A lower bound for the intrinsic velocity β can be derived from the observed jet to counterjet brightness ratio, assuming zero (or small) inclination of the jet of the LOS, which gives $\beta > 0.3$. The precessing beam model gives a jet to counterjet brightness ratio of 30. The discrepancy can be reduced if we assume the jets are intrinsically asymmetric; in fact, the northern

Table 3. 1928 + 73 1.3 cm-VLBI components 1985.10–1989.73

Comp.	S (Jy)	R (mas)	±	p.a.(°)	±	Size <i>a</i> (mas) × <i>b</i> (mas)	φ(°)	Epoch
A	0.7					0.33 × <0.1	159	1985.10
	1.1					0.25 × <0.1	146	1986.40
	1.12					0.25 × <0.1	146	1987.44
	1.29					0.35 × <0.1	147	1988.73
	1.04					0.27 × <0.1	151	1989.25
	0.85					0.30 × <0.1	153	1989.71
B	0.3	0.4	0.1	151	5	0.2 × <0.1	129	1985.10
	0.2	0.55	0.1	164	6	0.2 × 0.15	148	1986.40
	0.37	0.7	0.2	165	10	0.29 × 0.18	131	1987.44
	0.19	1.3	0.1	160	2	0.31 × 0.15	146	1988.73
	0.23	1.6	0.2	162	3	0.7 × 0.2	176	1989.25
	0.07	1.70	0.2	161	3	0.3 × 0.2	—	1989.71
C	0.7	0.64	0.05	164	1	0.2 × <0.1	146	1985.10
	0.6	1.06	0.05	165	2	0.2 × 0.15	142	1986.40
	0.69	1.33	0.1	162	2	0.33 × 0.24	125	1987.44
	0.28	1.81	0.05	160	2	0.44 × 0.12	101	1988.73
	0.22	2.05	0.05	158	3	0.37 × 0.19	75	1989.25
	0.19	2.18	0.1	161	2	0.57 × 0.12	81	1989.71
D	0.1	1.3	0.3	167	5	0.7 × 0.2	135	1985.10
	0.2	1.5	0.3	167	5	0.7 × 0.2	139	1986.40
E	0.2	2.3	0.4	161	10	0.8 × 0.8	—	1985.10
A1	0.64	0.69	0.05	167	1	0.27 × <0.1	7	1988.73
	0.62	0.90	0.05	169	1	0.19 × 0.11	0	1989.25
	0.48	0.96	0.1	170	1	0.25 × 0.12	9	1989.71
A2	0.61	0.46	0.05	150	2	0.34 × <0.1	2	1989.25
	0.72	0.47	0.1	146	2	0.22 × <0.1	20	1989.71

lobe is about 3 times brighter than the southern lobe, as can be derived by summing the flux densities within the circles superimposed on the lobe positions in Fig. 2 (see also Sect. 3.5). Asymmetry of the lobe intensities could be the result of an asymmetric energy flow in the jets, which, in the case of equal efficiency, should then lead to different jet intensities. Another possible explanation for the discrepancy might be the existence of a boundary layer in the jet, giving rise to a velocity gradient across the jet diameter. For this case Komissarov (1990) found that the brightness ratio of the jet and counterjet should be significantly smaller than in the “standard” model (for the velocity profiles analyzed by Komissarov, a factor of roughly 6 with $i = 1$ rad and Lorentz factor $\gamma = 10$).

From the spectral index analysis (see Sect. 3.5) we derive a spectral index of the northern lobe of $\alpha_{1.5\text{ GHz}}^{5\text{ GHz}} = -0.9$. Assuming the spectrum to have the same spectral index down to 408 MHz, but using a steeper slope of -1 above 5 GHz up to the adopted high frequency cut-off at $2 \cdot 10^{14}$ Hz, we calculate a bolometric (400 MHz– $2 \cdot 10^{14}$ Hz) luminosity of the extended lobe flux within the circles (thus ignoring the contribution from the halo) of $\approx 5 \cdot 10^{42}$ erg s $^{-1}$. This is about 100 times less than the hot spot luminosity found in the radio galaxy Cygnus A by Muxlow et al. (1988). Despite the comparatively low lobe luminosity of 1928 + 738, the core luminosity is about 30 times higher than the

luminosity of the core of Cygnus A (3.26 Jy at 6 cm, $z = 0.057$; Perley et al., 1984), consistent with the presence of strong Doppler-boosting in the core of 1928 + 738.

As can be seen from the high resolution 408 MHz MERLIN map [which shows structures very similar to those in the high resolution VLA map by Johnston et al. (1987)] and the MERLIN map at 18 cm, the southern jet is remarkably straight until it is “deflected” at about 8 arcsec south of the core (see Sect. 3.5). This feature is difficult to explain with the simple precessing beam model, which predicts a smoothly curved jet close to the core (e.g. Fig. 1). As the line in Fig. 3b shows, a more complex model, featuring a decreasing velocity (from $\beta = 0.9$ to $\beta = 0.6$) along the jet is able to explain the straight jet line near the core, if the azimuth angle is 150° .

3.2. Relativistic beaming on the mas scale

At 1.3 cm wavelength, 1928 + 738 displays a very pronounced bright jet on the mas scale. In Fig. 5, we aligned the 1.3 cm maps relative to the core, which is the northernmost, most compact and usually the brightest component in the maps. Furthermore, the core component has a flat spectral index between 1.3 and 3.6 cm, whereas the jet components have steep spectra, as shown by an observation of 1928 + 73 at 3.6 cm (Schalinski et al., in prep.). The

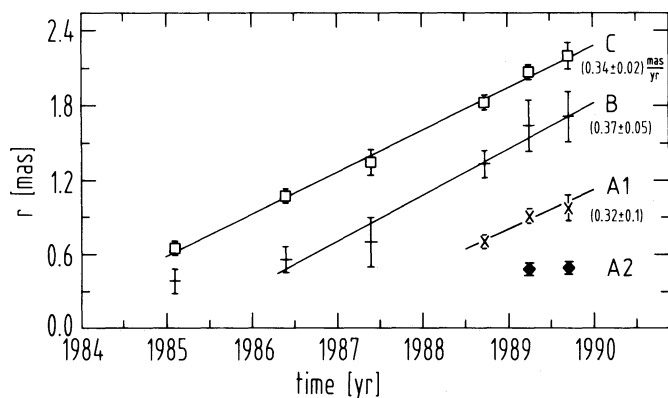


Fig. 6. Separations of the components from the core, derived from model fitting, plotted versus time

map of epoch 1989.71 has been shifted southward (0.1 mas) in order to account for a possible shift in the core position (see below). An identification of the components between epochs, indicated in Fig. 5, is first of all suggested by the motion of component C (straight dashed line). This peculiar component was elongated perpendicular to the jet in the last 3 epochs and is thus easily identifiable in the maps. It follows that at the first epoch, the strongest component was actually component C. This identification leads to a proper motion of $\mu = 0.34 \pm 0.03$ mas yr⁻¹, corresponding to an apparent velocity of $4.0 \pm 0.4c$. The values for the individual components are (see also Fig. 6) C: $\mu = 0.34 \pm 0.02$ mas yr⁻¹, B: $\mu = 0.37 \pm 0.05$ mas yr⁻¹ (not using the position measured in 1985.1 which indicates possible acceleration), A1: $\mu = 0.32 \pm 0.10$ mas yr⁻¹. In Fig. 5, component B does not seem to fit this scheme at epoch 1987.44; however, the data for this observation are considerably worse than at the other epochs and, in particular, lack long baselines, so that we do not consider this result as a serious objection to the scheme. In fact, a formal error analysis of the corresponding parameters derived by model-fitting, as well as a “maximum entropy” image (Caltech VLBI software, task VLBMEM), showed this component to be poorly defined and strongly elongated along the jet axis.

In the calculations above we assumed that the core is stationary. Any slight change in the apparent core position is attributed to blending with an emerging new component. To derive estimates for these shifts we fitted Gaussian profiles to slices across the core position (position angle p.a. = 165° along the jet) in the 1988.73 and 1989.25 maps. As can be seen from Fig. 7a and 7b, the broad profile at epoch 1988.73 can be interpreted as the blending of two unresolved (FWHM equal to the beam width) components, which are clearly separated at 1989.25. A shift of the peak brightness position between these two epochs of 0.03 mas, less than a fifth of the beam, was derived. However, if an emerging new component is very bright with respect to the core, the shift can be larger. The core profile along the jet at epoch 1989.71 is significantly asymmetric, so that a shift of the brightness centroid down the jet is very probable. We think that a blend of the core emission with that of a new, strong emerging component may have corrupted the apparent position of the core. We do not consider the alternative possibility that the motion of the components has stopped suddenly to be a reasonable scenario.

Schalinski (1990) and Schalinski et al. (1991) reported that the quasar 1928 + 738 displays superluminal motion of components

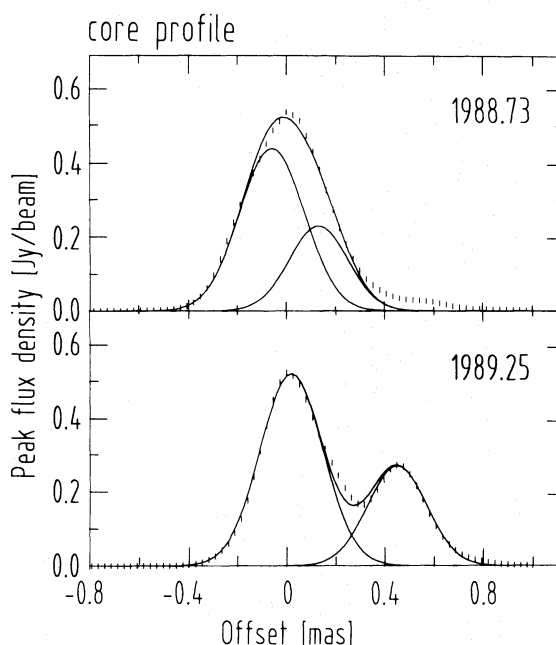


Fig. 7. Decomposition of the core profile at $\phi = 165^\circ$ at epochs 1988.73 (upper) and 1989.25 (lower). Measured profiles (bars), and Gaussian profiles and their sums (lines) are drawn

at 6 cm with a mean velocity of $(6.5 \pm 0.5)c$. Thus, we have detected acceleration between scales of ≈ 2 mas and 6–15 mas. Apparent acceleration has been reported for other sources (e.g. 3C 345; Biretta et al. 1986).

The small brightness difference of jet and counterjet on arcsecond scales is not expected from the superluminal motion on the mas scale. Given the apparent velocity of $4c$ ($6c$) of the jet components, the mas scale jet cannot be inclined by more than 28° (19°) to the LOS. Thus, within the first few arcseconds from the core, the jet either has to bend by more than 50° on both sides of the core, or the bulk Lorentz factor has to decline from about $\gamma = 7$ to $\gamma = 1.08$, the latter value corresponding to an intrinsic velocity of $0.4c$. Even if both effects are present at the same time, the necessary changes are not much less dramatic. There is no obvious evidence in the data of such considerable changes either in the viewing angle or the bulk Lorentz factor γ within that region.

In the precessing beam model, the angle of the jet to the LOS varies in the range $i \pm \psi$. For counterclockwise precession, the angle of the jet to the LOS at the core of 1928 + 738 is close to its minimum of $i - \psi \approx 35^\circ$. The position angle is $\approx 170^\circ$, consistent with the position angle of the VLBI jet. Further down the jet, the angle to the LOS increases to its maximum values of $i + \psi \approx 51^\circ$ near component 4. The position angle of the jet gradually changes from 170 to 190° at a few arcseconds distance from the core, consistent with the observed behaviour (but see Sect. 3.1).

Since the difference between the lowest possible inclination of the mas scale jet of the models and the largest inclination allowed by the observed apparent velocity is of the order of 10° , we suggest that the visible mas jet is only a filament in a jet which is actually broader (see also Johnston et al. 1987). In the “broad beam” concept (e.g. Daly & Marscher 1988), strong Doppler favouritism greatly enhances the parts of a relativistic jet lying closer to the LOS so that they dominate over other parts, given the relatively

low dynamic range of the VLBI maps at 22 GHz. Very high dynamic range VLBI maps should be made to check on this concept. Furthermore, the apparent incompatibility of the smooth jet line of the model with the distorted mas scale jet is not a particular problem of the model on these scales, since the jet on arcsecond scales cannot yet be mapped with the same resolution and similar wiggles should also be present on these scales.

3.3. Kinematics on the sub mas to mas scale

According to Begelman et al. (1980), the Lense–Thirring effect may align jets with the rotation axis of the central black hole. In the presence of an orbiting secondary black hole, the rotation axis undergoes precession (e.g. with a period of 400 000 yr for 1928 + 738). The 1.3 cm VLBI observations show a strikingly continuous and regular transverse oscillation of the jet (a “wave”) which might be interpreted as being due to orbital motion perpendicular to the jet axis (with a period of a few years) of the more massive component in a binary black hole system. One specific prediction of this model is motion of the components of the jet (e.g. those visible in the 1.3 cm maps) on parallel ballistic trajectories away from the core (whose position oscillates perpendicular to the jet direction). Motivated by this reasoning, we use the VLBI observations to investigate in this section the kinematics of the wave in more detail. In the next section we shall interpret and examine parameters in the framework of the model.

Two approaches can be used: first, the study of the motion of the components used in the model fitting procedure as a representation of the jet, and second, the study of the jet ridge line over its complete extent, calculated from transverse slices across the maps.

From Fig. 8 we conclude that, within the errors, none of the components changed their position angle p.a., except component B. We show in Figs. 8 and 9 that this does not necessarily imply non-ballistic motion for component B, since an offset of the line of motion of component B of only 0.1 mas from the core would result in the observed change in position angle. A similar interpretation could be used to explain the position angle change of component 4 in the jet of quasar 3C 345, reported by Biretta et al. (1986).

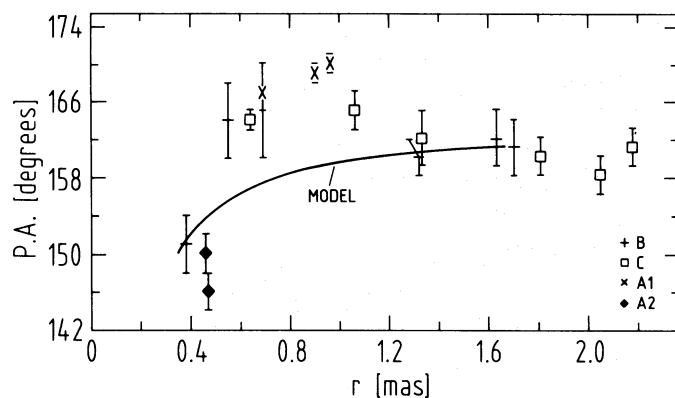


Fig. 8. Position angles of the Gaussian components with respect to the core, derived from model fitting. The curved line corresponds to a hypothetical component moving along the straight line superimposed on the true path of component B (see Fig. 9)

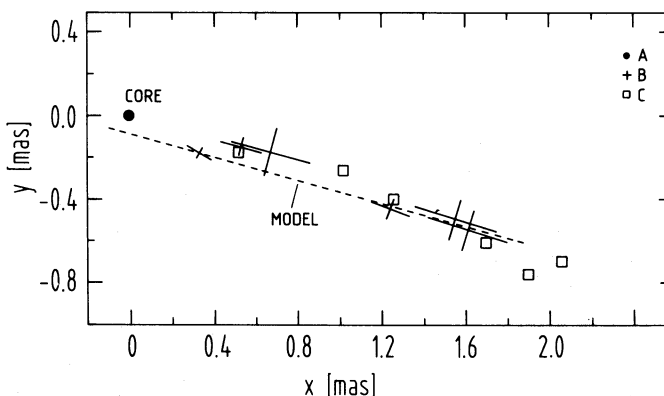


Fig. 9. True paths of components B and C. The dashed line corresponds to the line in Fig. 8 and assumes a straight path for the motion of B

Since component flux densities can change, leading to shifts in the brightness centroids in a continuous jet, we used the second approach to increase the significance of kinematical interpretations. In order to benefit from the whole jet line, we chose sine wave fitted to them since this class of curve provides good fits to the jet lines, especially those of 1988.73 and 1989.25 (except for the part of the jet next to the core, especially in 1987.44 and 1989.71, see Sect. 3.6). Although this restricts the possible kinematical models we will show that it gives a consistent description of one of them.

The maps were restored with a beam of 0.1 mas in order to prevent the transverse oscillation from being smeared out (Fig. 10); the resulting lack of smoothness of the jet line is compensated by the fitting procedure. Parameters of the sine waves are as follows: amplitude A , wavelength λ , phase ϕ and two coordinates describing the relative position on the sky, offset o and rotation angle r . For the jet lines of 1988.73 and 1989.25, the fitted sine waves (all parameters allowed to vary) happened to yield almost the same values for the parameters, except for the phase (1988.73: $A=0.09$ mas, $\lambda=1.06$ mas, $\phi=175^\circ$; 1989.25: $A=0.10$ mas, $\lambda=1.07$ mas, $\phi=129^\circ$). The phase shift translates into a shift of 0.14 mas, corresponding to 0.27 mas yr^{-1} . This result is consistent with motion of the parts of the jet on parallel ballistic trajectories, therefore preserving its shape. We then fitted sine waves to the jet lines at the other epochs (except 1986.40), whereby o and r , as well as λ were taken from the well defined jet lines we started with. From Fig. 10 it can be seen that the sine waves fit reasonably well, although at epoch 1987.44 for example, a sine wave with a smaller amplitude would fit equally well. The quality of the data does not yet allow to introduce an additional free parameter related to increasing amplitudes and diverging trajectories; it is, however, expected to be of small value. The jet line in the map of 1986.40 is poorly defined, but this map was made from data with a poor aperture plane coverage (snapshot data).

From Fig. 10, we derive a proper motion $\mu \approx 0.28 \pm 0.05 \text{ mas yr}^{-1}$ of the sine wave consistent with all epochs (except 1989.71, see below), within the errors (crude estimates for the phase errors were derived from the range of phases corresponding to less than 2 times the standard deviation of the best fit at each epoch). This proper motion also equals that derived above for the jet components, indicating that there is no significant motion of the components with respect to the sine wave. We did not use the data

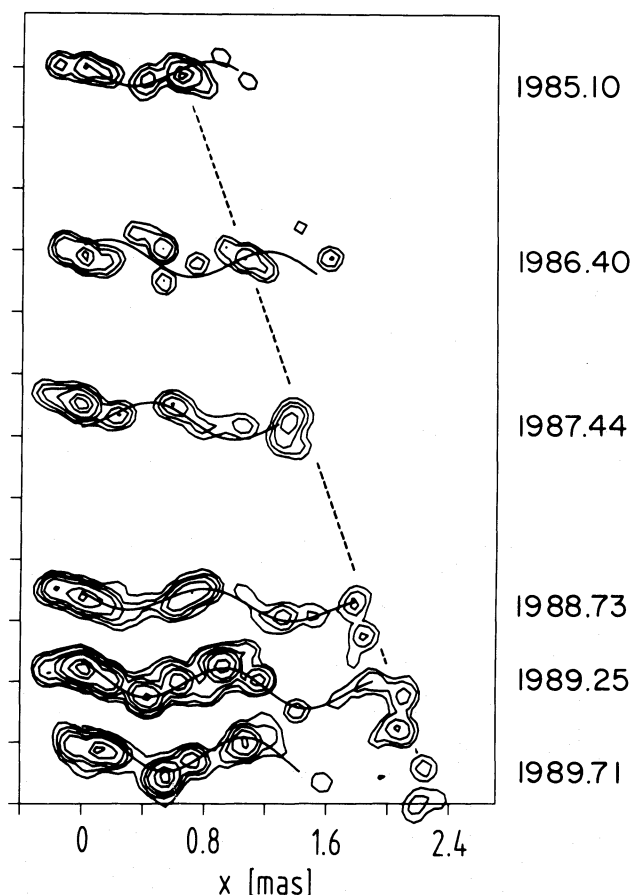


Fig. 10. Display of maps at 0.1 mas resolution, drawn with fitted “sine waves” (see Sect. 3.3). Core position is fixed along the vertical axis. The oblique dashed line connects the positions of component C at the various epochs and has a slope of 0.34 mas yr^{-1} . Contour levels of the maps are at epoch 1985.10, 1986.40: 5, 10, 20, 50, 80% of the peak flux density; at epochs 1987.44, 1988.73, 1989.71: 2, 5, 10, 20, 50, 80%; at epoch 1989.25: 1, 2, 5, 10, 20, 50, 80%. Note that the “sine wave” for epoch 1986.40 does not fit the jet line well (see text). This may be the result of the significantly worse aperture plane coverage at this epoch compared to the other epochs, which has yielded a map of lower quality

of epoch 1989.71 in the derivation of the sine wave motion, since the core position was probably ill defined. However, this epoch is well suited to yield an argument against non-ballistic motion along a path defined by the sine wave of epoch 1988.73, if one considers the relative position angle of the components A1 and A2. Given non-ballistic motion following the jet ridge line of epoch 1988.73, this angle should have changed by -16° , owing to the favourable relative position of these components with respect to the sine wave. Actually, it has not changed ($+2^\circ \pm 6^\circ$). We therefore conclude that the “moving sine wave” model gives a good description of the kinematics of the jet. It agrees with the kinematic predictions by the binary black hole hypothesis.

3.4. Parameters of a hypothetical binary black hole system

In this section we adopt the binary black hole model and calculate some relevant parameters in order to judge whether this model implies physically reasonable results. The observed orbital period (equal to λ/μ) is 3.8 yr, which corresponds to 2.9 yr in the

rest frame of the source. The amplitude of the wiggle is 0.3 pc; this value however, is too large to be interpreted as the binary separation since it would imply superluminal circumferential motion. Adopting a mass of the primary black hole of $10^8 M_\odot$ which would be sufficient (on the basis of the Eddington limit) to account for the luminosity of 1928 + 738 ($8.5 \cdot 10^{45} \text{ erg s}^{-1}$ uncorrected for boosting), we calculate, using formulae as given by Begelman et al. (1980), the separation to be 0.005 pc. If the mass of the secondary black hole is somewhat less than a hundredth of the mass of the primary, the observed precession period is reproduced. It is very unclear how jets can be produced in a very close binary system of black holes, what distortions they suffer when leaving that system and whether projection effects play a role in the apparent properties of the sinusoidal wiggle.

3.5. Interaction of the jet with ambient medium on arcsecond scales

As we have seen, the southern jet is straight for the first few arcseconds from the core, in a position angle ($+180^\circ$) in which the first counterjet component also appears [the faint blob next to the core in the VLA map (Fig. 1)]. The curved appearance of the southern jet therefore might be due to a deflection of the jet by a dense intergalactic cloud at component 3 (at a projected distance of 24 kpc from the core; projected deflection angle $\approx 45^\circ$), after which the jet comes to rest at a hot spot, to be identified with component 5. Kollgaard et al. (1990) have used polarization observations as evidence that component 5 might indeed be a hot spot. From the spectral index analysis we find that the high frequency spectral index of the southern jet (components 3, 4 and 5) is considerably flatter than the low frequency spectral index, which might be due to the presence of two components of emission in the southern jet. Component 2, at 5 GHz, seems to have a lower brightness than other components of the southern jet. This would make the high frequency spectral index of component 2 steeper than those of components 3, 4 and 5. Although it seems plausible that the jet brightens again, with a flatter spectrum, when interacting with an ambient medium at component 3, spectral information over such small frequency range is not sufficient to draw firm conclusions.

On the northern side, the jet already shows the first of several deflections before reaching component 6. This component exhibits a spectrum with indices $\alpha_{408 \text{ MHz}}^{1.5 \text{ GHz}} = -0.6$ and $\alpha_{1.5 \text{ GHz}}^{5 \text{ GHz}} = -0.5$. For relativistic beaming and a Doppler factor of 1.7 (as discussed above), the low frequency spectral index of component 6 (on the counterjet side) has to be compared to the high frequency spectral index of component 5 on the jet side, and thus is significantly steeper than the latter.

Since it seems unlikely that deflections (or possible Kelvin–Helmholtz instabilities) occurring as described above could lead to the observed symmetric source structure, we propose that the jets have been restarted after a quiescent phase and are now being deflected at the old lobes which remained from previous phases of activity (see e.g. Bridle et al. 1989).

3.6. Interaction of the jet with ambient medium on mas scales

Recent observations of pc-scale radio jets at high resolutions (especially at 7 mm, e.g. Krichbaum 1990b) have shown that strong jet curvature tends to be observed near the cores of the sources. Krichbaum et al. (1990) report partial sinusoidal oscillations in the jet of the quasar 3C 273 which might be related to a

helically bent jet. In the case of the quasar 3C 345, motion on different paths has been reported by Zensus (1990). These paths seem to be straight near the core, but do not intersect the core position so that position angle changes occur when the components move away from the core. At distances larger than ≈ 1 mas the paths are curved. Hardee (1981) presented a model for 3C 345 based on helical perturbations of a jet unstable against Kelvin–Helmholtz instabilities, which explains motion of components on curved trajectories.

To assess possible explanations of the oscillating ridge line of the jet of 1928 + 738 further, we note that the jet components are situated at the turning points of the ridge line (“alternate brightening”), as can be seen most obviously in the maps of the last three epochs. The rate of emergence of new components was about one every 1.6 years during our monitoring program, but may not be connected to periodic activity of the central engine. As we have seen above, the components do not follow the ridge line, but rather seem to move on parallel paths at the pattern speed of the sine wave, thereby maintaining the characteristic, alternately brightened structure. Since the pattern moves at superluminal speed, we conclude that the generalized model of oblique reflection mode shocks in a helical mode does not provide a ready explanation, because it predicts side-to-side (curved) motion of the components in a stationary pattern (Hardee & Norman 1989).

In the case of helically twisted filaments moving at a velocity close to the speed of light, differential Doppler boosting in a conical jet is required to transform the helical geometry into the apparent sinusoidal oscillation of the jet line of 1928 + 738 (see for example Fig. 2 in Gower et al. 1982). Depending on the angle of the jet to the LOS, the structure of the filaments and their apparent motion might be very complex. Rather than being due to fluid dynamical instabilities, helical filaments might be due to helical magnetic field structures in the jets. Various authors have described models in which magnetic field lines originate in a rotating magnetosphere anchored in an accretion disk and are therefore twisted helically (Uchida & Shibata 1985; Coroniti 1985). In this model, particles are accelerated by the “magnetic slingshot” effect to relativistic velocities when they cross the region near the light cylinder radius, at some hundred Schwarzschild radii, where the magnetic field lines bend from being parallel to the disk to being parallel to the rotation axis (Camenzind 1989; see also Uchida & Shibata 1986). The radii of curvature of the magnetic field lines grow to much larger values when the jet expands in a transition region; thus, a superluminal *phase* velocity, rather than a *physical* circumferential velocity, is associated with the ratio of the wavelength to the “orbital” period of the sine wave. The speed of advance of the magnetic field structure (the Alfvén speed) must be of the order of the speed of light in order to produce the observed apparent superluminal motion. The extrapolation of the sine wave to the core at several epochs misses the core position by roughly the value of the amplitude and might indicate the transition region. We note that the mean position angle of the elongated core component is inclined to the jet axis by about $12 \pm 5^\circ$ and may indicate different mechanisms of jet collimation. Observations at higher frequencies (e.g. 7 mm) are needed to investigate the trajectories of components just emerging from the core.

We further note that the amplitude of the sine wave is too small to be visible in VLBI maps at e.g. 6 cm (resolution ≈ 1 mas; see Witzel et al. 1988). However, ballistic component motion at a velocity of $4c$ in a straight jet is consistent with new results up to a

distance of 4 mas from the core; this distance marks the onset of higher component velocities ($\approx 6.5c$) and a different lateral jet oscillation pattern (Schalinski et al. 1991), indicative of a different physical process at work.

4. Summary and conclusions

On kpc scales, the quasar 1928 + 738 displays two-sided jet emission feeding two symmetrically placed lobes. The ratio of the lengths of jet and counterjet is consistent with the brightness ratio if interpreted as being due to relativistic beaming. The curved jets have been modeled with a relativistic precessing beam model featuring a cone opening angle of 20° , an inclination of 40° to the line of sight, a precession period of 400 000 yr and an intrinsic velocity of $0.7c$. The observed jet to counterjet brightness ratio is explained to within a factor of 3, which however, is of the same order as an observed brightness asymmetry in the lobes.

On pc scales, 1928 + 738 displays a pronounced one-sided jet. VLBI observations at 1.3 cm have detected component motion at a speed of $4c$, which is significantly slower than observed further down the jet at 6 cm ($6.5 \pm 0.5c$). The inclination of the jet to the line of sight at the position of the core predicted by the precessing beam model is inconsistent with the observation of apparent superluminal motion and it has been concluded that the VLBI jet might consist of Doppler-boosted filaments in a broad jet.

On sub-mas scales, the jet undergoes a regular wiggle (“sine wave”) with an amplitude of 0.1 mas (0.3 pc). The components seem to move along parallel ballistic trajectories, rather than along a fixed path coinciding with the curved ridge line of the jet. The possibility that these motions could be due to orbital motion in a binary black hole system (which could, in addition, lead to jet precession) has been investigated. It is concluded that the implied binary separation (0.3 pc) would, however, be too large. Another, possibly more realistic, scenario involving helically twisted magnetic field lines in an expanding conical jet has been presented.

Acknowledgements. We would like to thank Dr. I.I.K. Pauliny-Toth for a critical reading of the manuscript. The efforts of the staffs of the participating observatories of the European and US VLBI networks are gratefully acknowledged. Thanks are due to H. Blaschke, H. Lüdeke and U. Stursberg for their patient help with the correlation. We also would like to thank the referee Dr. R.T. Schilizzi for comments and carefully reading the manuscript.

References

- Alef W., Porcas R.W., 1986, A&A 168, 365
- Begelman M.C., Blandford R.D., Rees M.J., 1980, Nat 287, 307
- Biretta J.A., Moore R.L., Cohen M.H., 1986, ApJ 308, 93
- Bridle A.H., Fomalont E.B., Byrd G.G., Valtonen M.J., 1989, AJ 97, 674
- Burns J.O., Christiansen W.A., 1980, Nat 287, 208
- Camenzind M., 1989, in: Belvedere G. (ed.) *Accretion Disks and Magnetic Fields in Astrophysics*. Kluwer, Dordrecht, p. 129
- Coroniti F.V., 1985, in: Kundu M.R., Holman G.D. (eds.) *Unstable Current Systems and Plasma Instabilities in Astrophysics*. Reidel, Dordrecht, p. 453
- Daly R.A., Marscher A.P., 1988, ApJ 334, 539
- Eckart A., Witzel A., Biermann P., et al., 1985, ApJ 296, L23
- Fiedler R.L., Henriksen R.N., 1984, ApJ 281, 554

- Gower A.C., Gregory P.C., Hutchings J.B., Unruh W.G., 1982, *ApJ* 262, 478
- Henriksen R.N., 1984, in: Bridle A.H., Eilek J.A. (eds.) *Physics of Energy Transport in Extragalactic Radio Sources*. NRAO, Greenbank, p. 122
- Henriksen R.N., Vallée J.P., Bridle A.H., 1981, *ApJ* 249, 40
- Hardee P.E., 1981, *ApJ* 259, L9
- Hardee P.E., 1987, *ApJ* 318, 78
- Hardee P.E., Norman M.L., 1989, *ApJ* 342, 680
- Hummel C.A., Schalinski C.J., Krichbaum T.P., Witzel A., Johnston K.J., 1988, *A&A* 204, 68
- Johnston K.J., Simon R.S., Eckart A., et al., 1987, *ApJ* 313, L85
- Kollgaard R.I., Wardle J.F.C., Roberts D.H., 1990, *AJ* 100, 1057
- Komissarov S.S., 1990, *Sov. Astron. Lett.* 16, 284
- Krichbaum T.P., 1990a, Dissertation, Rheinische Friedrich-Wilhelms-Universität zu Bonn
- Krichbaum T.P., 1990b, in: Zensus J.A., Pearson T.J. (eds.) *Parsec-scale Radio Jets*. Cambridge University Press, Cambridge, p. 83
- Krichbaum T.P., Booth R.S., Kus A.J., et al., 1990, *ApJ* 237, 3
- Kühr H., Witzel A., Pauliny-Toth I.I.K., Nauber U., 1981, *A&AS* 45, 367
- Lawrence C.R., Pearson T.J., Readhead A.C.S., Unwin S.C., 1986, *AJ* 91, 494
- Lawrence C.R., Readhead A.C.S., Pearson T.J., Unwin S.C., 1987, in: Zensus J.A., Pearson T.J. (eds.) *Superluminal Radio Sources*. Cambridge University Press, Cambridge, p. 260
- Lonsdale C.J., Barthel P.D., 1984, *A&A* 135, 45
- Lupton R.H., Gott III J.R., 1982, *ApJ* 255, 408
- Muxlow T.W.B., Pelletier G., Roland J., 1988, *A&A* 206, 237
- O'Dea C.P., Owen F.N., 1987, *ApJ* 316, 95
- O'Donoghue A.A., Owen F.N., Eilek J.A., 1990, *ApJS* 72, 75
- Perley R.A., Dreher J.W., Cowan J.J., 1984, *ApJ* 285, L35
- Roos N., 1988, *ApJ* 334, 95
- Rusk R., Rusk A.C.M., 1986, *Can. J. Phys.* 64, 440
- Schalinski C.J., 1990, Dissertation, Rheinische Friedrich-Wilhelms-Universität zu Bonn
- Schalinski C.J., Witzel A., Hummel C.A., et al., 1991, *Proc. Workshop on Variability of AGN*, Turku, Finland, January 1991 (in press)
- Uchida Y., Shibata K., 1985, *PASJ* 37, 515
- Uchida Y., Shibata K., 1986, *Can. J. Phys.* 64, 507
- Witzel A., 1987, in: Zensus J.A., Pearson T.J. (eds.) *Superluminal Radio Sources*. Cambridge University Press, Cambridge, p. 83
- Witzel A., Schalinski C.J., Johnston K.J., et al., *A&A* 206, 245
- Zensus J.A., 1990, in: Zensus J.A., Pearson T.J. (eds.) *Parsec-scale Radio Jets*. Cambridge University Press, Cambridge, p. 28